PCCP

Inferring Networks of Chemical Reactions by Curvature Analysis of Kinetic Trajectories

Journal:	*Physical Chemistry Chemical Physics*
Manuscript ID	CP-ART-11-2024-004338.R1
Article Type:	Paper
Date Submitted by the Author:	04-Feb-2025
Complete List of Authors:	Narayanan, Vignesh; University of South Carolina Bordoh, Lawrence K.; Saint Louis University Kiss, Istvan; Saint Louis University Li, Jr-Shin; Washington University in St Louis

Journal Name

ARTICLE TYPE

Cite this: DOI: 00.0000/xxxxxxxxxx

Inferring Networks of Chemical Reactions by Curvature Analysis of Kinetic Trajectories†

Vignesh Narayanan,[a]‡ Lawrence K. Bordoh,[b]‡ István Z. Kiss,*[b]‡ and Jr-Shin Li[c]‡

Received Date
Accepted Date

DOI: 00.0000/xxxxxxxxxx

Quantifying interaction networks of chemical reactions allows description, prediction, and control of a range of phenomena in chemistry and biology. The challenge lies in unambiguously assigning contributions to changes in rates from different interactions. We propose that the curvature change of kinetic trajectories due a systematic perturbation of a node in a network can identify the coupling strength and topology. Specifically, the coupling strength can be calculated as the ratio of the curvature change measured from the coupled node and the rate change of a perturbed node. We verified the methodology in numerical simulations with a network with complex ordinary differential equations and experiments with electrochemical networks. The experiments show excellent network inference (without false positive or negative links) of various systems with large heterogeneity in local dynamics and network structure without any a-priori knowledge of the kinetics. The theory and the experiments also clarify the influence of local perturbations on response amplitude and timing through network-wide up-regulation. A major advantage of our technique is its independence from hidden/unobserved nodes. This makes our method highly suitable for applications with high temporal and low spatial resolution data from interacting chemical and biochemical systems including neuronal activity monitoring with multi-electrode arrays.

1 Introduction

Networks in chemically reacting systems underlie functionality at various scales, such as chemical species forming reactions, chemical reactions interacting in discrete units such as in biological cells, or chemical products made in networks of factories[1,2]. Identifying the topology and the functional form of such interactions are important steps for modeling in reaction kinetics[3], with wide range of applications in biochemistry, such as cellular metabolism[4] and signal transduction pathways[5], in advanced industrial applications in catalysis[6], combustion[7], polymerization[8], atmospheric chemistry[9], and testing hypotheses about the origin of life[10]. The topology of chemical reaction networks has important impact on its functionality; it determines the concentration response patterns[11–13] and other critical aspects such as the rate laws, the multiplicity of steady states, and the nature of dynamic instabilities[14–16]. Similarly, when discrete chemical reaction units are coupled in networks[17–19], the toolkit of network science can be used to explain the formation of isolated reaction domains[20] and various forms of synchronization patterns that include emergence of coherence[21,22], clustering[23,24], and chimeras[25–27]. These processes play an important role in the morphogenesis (with Turing patterns in networks[28]) and the functioning of biological clocks and pacemaker cells[29].

Nonetheless, inference of reliable networks from experimental data poses many challenges. Statistical models use metrics such as mutual information and correlation[30–34] while systems-theoretic approaches infer the kinetic models by fitting nonlinear models[29,35–37]. The major challenge is separating local dynamics from the impact of directly and indirectly coupled units and obtaining reliable connections from limited measurements, for example, when some species/units are hidden. To overcome the problem that many (often dissimilar) models can describe experimental data, perturbation-based methods were developed to infer functional connections[38,39]. For example, up-regulation of gene expressions or enzyme concentrations can be used to explore network topology by assessing the rate of change over time or by fitting the time series data to the response[38–40]. Yet, similar limitations arise because it is difficult to design an experiment that guarantees data sufficiency for identification of species/unit interactions.

In this paper, we propose that an analysis of the curvature of the kinetic trajectories (i.e., second derivative of concentration with respect to time) provide a definite solution to infer the topology

[a] AI Institute, University of South Carolina, 1112 Greene St, Columbia, SC 29208.
[b] Department of Chemistry, Saint Louis University, 3501 Laclede Ave, St. Louis, MO 63103.
[c] Department of Electrical and Systems Engineering, Washington University in St. Louis, 1 Brookings Dr, St. Louis, MO 63130.
E-mail: istvan.kiss@slu.edu. *Corresponding author.

† Supplementary information available: [details of any supplementary information available should be included here]. See DOI: 00.0000/00000000.

‡These authors contributed equally to this work.

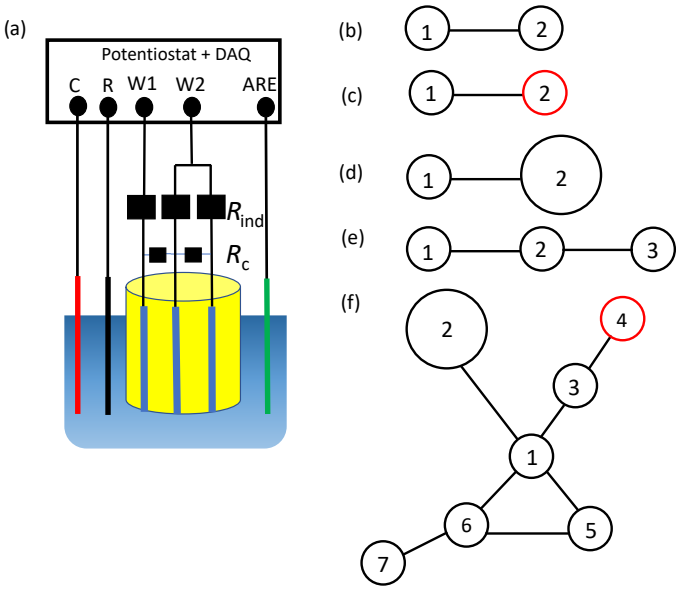

Fig. 1 Experimental setup and coupling topologies. (a) Schematic diagram of a three-electrode electrochemical cell with a counter (C), a reference (R), and multiple working electrodes connected to the two working points ($W1$ and $W2$) of a bipotentiostat. R_{ind}: individual resistance, R_c: coupling resistance. ARE: Auxiliary reference electrode used for measuring the electrode potentials. Right column: Considered topologies. (b) Two coupled electrodes with the same size and same individual resistance (coupling of units with nearly identical dynamics). (c) Two coupled electrodes with the same size but different individual resistance (coupling of units with different dynamics) (d) Two coupled electrodes with different electrode sizes. (e) Three electrodes in a chain. (f) Complex network topology with different electrode sizes. Red circle denotes heterogeneous node (with different individual resistance than the rest).

and the strength of interactions in dynamical reaction networks even without a-priori knowledge of the kinetics and in the presence of hidden and/or unobserved units.

First, we develop a theory that shows that coupling strengths can be calculated by comparing the curvature change in the kinetic trajectories due to a step perturbation of a (localized) parameter in the kinetic equations. Then, the technique's effectiveness is validated through numerical reconstruction of a network of the highly nonlinear Lorenz system. The technique is tested in experiments with networks of coupled electrochemical reactions, where the role of the strength and symmetry of coupling as well as the heterogeneity of local dynamics can be explored. The application of the theory also reveals how measuring both the time-scale and extent of the network response due to up-regulation can be used to quantify the coupling.

2 Experimental Methods

A standard electrochemical cell consisting of a multiple nickel working electrodes (Goodfellow Cambridge Ltd, 99.98%), a Hg/Hg_2SO_4/saturated K_2SO_4 reference electrode (640 mV electrode potential vs. standard hydrogen electrode), and a 1.57 mm diameter titanium rod coated in platinum counter electrode in 3 mol/L sulfuric acid were used in this experiment. A schematic of the experimental setup is shown in Fig. 1a. An auxiliary reference electrode (ARE) was added to measure the electrode potentials using chronopotentiometry. The working electrode was made of 2-7 wires that can have identical diameters for symmetrical, or different diameters for asymmetrical coupling depending on the coupling topology under investigation. The wires were embedded in epoxy with at least 3 mm spacing between them; the relatively large separation diminishes electrical and mass transfer coupling through the electrolyte. The reactions take place only at the end of the exposed area, which is wet polished on a series of sandpapers (P180 - P4000) with a Buehler Metaserv 3000 polisher. All the experiments were carried out at 10 ^{o}C, maintained by a Neslab RTE-7 circulating bath. External individual resistances, R_{ind} (with typical values of 5 to 15 kohm), were added to each electrode.

The electrode arrays were connected to a Pine Instrument AFCBP1 bipotentiostat with the perturbed electrode connected to W1 (working electrode port 1) and all the coupled electrodes connected to W2 (working electrode port 2) of the bipotentiostat. The experimental setup was then interfaced with a real-time LabVIEW controller to measure the electrode potentials $E_p(t)$ and $E_c(t)$ at 10 kHz and to set the circuit potential $V_j(t)$ of the wires. Throughout the experiments, we set the circuit potential to $V =$ 0.9 V which was then perturbed through a step function to 1.1 V. The coupling resistances R_c, which varied between 1-100 kohm, were introduced between Ni electrodes in order to induce coupling. Comprehensive results for all the experiments are reported in SI Section 4.

3 Results and Discussions

3.1 Theory

To validate the theory, we consider two coupled kinetic equations for two species/dynamical units denoted as x_p, the perturbed unit, and x_c the coupled unit. Each unit has its own rate equations f and g, respectively, and the rate equation of x_p can be addressed individually through a parameter α. The system thus can be described by rate equations

$$\dot{x}_p = f(x_p, \alpha), \tag{1}$$

and

$$\dot{x}_c = g(x_c) + K(x_p - x_c), \tag{2}$$

From time series data at the beginning ($t = 0$) of the procedure when the parameter $\alpha = \alpha_1$, the state of the perturbed and coupled units are x_p^* and x_c^*, and thus the corresponding rates are

$$\dot{x}_p(0) = \dot{x}|_{x_p^*, \alpha_1} = f(x_p^*, \alpha_1), \tag{3}$$

and

$$\dot{x}_c(0) = \dot{x}|_{x_c^*, x_p^*} = g(x_c^*) + K(x_p^* - x_c^*). \tag{4}$$

and thus the curvature of the kinetic trajectory of the coupled unit is

$$\ddot{x}_c(0) = \frac{dg}{dx_c}\, \dot{x}_c|_{x_p*, x_c*} + K(\dot{x}_p|_{x_p^*, \alpha_1} - \dot{x}_c|_{x_c^*, x_p^*}). \tag{5}$$

For $t > 0$, the x_p unit is perturbed by setting $\alpha = \alpha_2$. The system remains in the same state, but from the kinetic trajectories after the perturbation, the rate of perturbed units is now

$$\dot{x}_p(0^+) = \dot{x}|_{x_p^*,\alpha_2} = f(x_p^*, \alpha_2). \quad (6)$$

Note that the rate of the coupled unit remains unchanged,

$$\dot{x}_c(0^+) = \dot{x}|_{x_c^*,x_p^*} = g(x_c^*) + K(x_p^* - x_c^*). \quad (7)$$

However, the curvature is now

$$\ddot{x}_c(0^+) = \frac{dg}{dx_c}\, \dot{x}_c|_{x_p*,x_c*} + K(\dot{x}_p\big|_{x_p^*,\alpha_2} - \dot{x}_c|_{x_c^*,x_p^*}), \quad (8)$$

By comparing Eqs. 5 and 8 we can see that the curvature change evaluated from the trajectories from before and after the perturbation of the coupled unit is related to the change of the rate measured from the perturbed unit, i.e.,

$$\Delta\ddot{x}_c = K\Delta\dot{x}_p, \quad (9)$$

where $\Delta\ddot{x}_c = \ddot{x}_c(0^+) - \ddot{x}_c(0)$ and $\Delta\dot{x}_p = \dot{x}_p(0^+) - \dot{x}_p(0)$. Using this equation, the coupling strength can be calculated as the ratio of the difference in the curvature and the slope change of the coupled and perturbed units, respectively:

$$K = \frac{\Delta\ddot{x}_c}{\Delta\dot{x}_p}. \quad (10)$$

Note that this formula for the coupling strength is independent of the local dynamics f and g (including the sensitivity of the local kinetics on the perturbation parameter α). This feature, i.e., independent recovery of coupling strengths from local dynamics, is crucial for reconstructing models that are computationally unambiguous and for assigning contributions to changes in rates from different interactions. Because the value of parameter α needs to be changed from α_1 to α_2 at $t = 0$, a natural choice for the perturbation is a step change. However, other waveforms could also be applied (e.g., square or pulse) that change the value of the parameter at $t = 0$. For simplicity, from hereon we assume a step perturbation. Also, the formulation presented here served as a representative simplified example through which the method can be explained; we also described the method from a general mathematical perspective to show that the proposed approach can be applied to a general class of nonlinear dynamic networks with highly nonlinear local dynamics with practically any type of network (see SI Section 1). We note, however, that we did make an important assumption that the coupling dynamics is linear. The method provides the coupling strength as the linear component of the coupling at the state of the local kinetics where the perturbation was applied. With nonlinear coupling, the method should be repeated at different states, and a coupling formula should be reconstructed based on the inferred, stated dependent, linearization of the coupling formula.

To implement Eq. (10) the following step-by-step protocol should be followed. Within a network, a unit k is perturbed, and the rate change is evaluated for the unit in the moment of the perturbation. The curvature change should be then calculated for all the other observed nodes. This way, the outgoing connections to all observed nodes can be calculated using Eq. (10). The method is not affected by the presence of nodes that are not observed (or hidden nodes) - the network links to those hidden nodes are simply not recovered but the lack of their observation does not have any effect on the inference of the observed units because they do not enter Eq. 10. Finally, the procedure should be repeated for perturbing any node for which the outgoing connections are needed. Thus, to recover all the connections in a network of N nodes, N step-perturbation experiments should be applied by perturbing each node in the subsequent experiments; for each experiment, the time series data of all the N nodes should be collected to evaluate the slope and curvature changes.

3.2 Validation with Numerical Simulations

The proposed idea is illustrated using a three-node chain network in Fig. 2. Node 1 is connected to node 2, and node 2 to node 3. Note that node 1 is not directly connected with node 3 (Fig. 2(a)). For local dynamics, we considered the highly nonlinear Lorenz system with parameters that correspond to damped oscillations to a stationary state as shown in Fig. 2(c)-(e).

The network of the 3 units are thus governed by the dynamic equations

$$\begin{aligned}
\dot{x}_i(t) &= \sigma(y_i(t) - x_i(t)) \\
\dot{y}_i(t) &= r x_i(t) - y_i(t) - x_i(t) z_i(t) + \sum_{j=1, j\neq i}^{N} K_{ij} y_j(t) + u_i(t) \\
\dot{z}_i(t) &= -b z_i(t) + x_i(t) y_i(t),
\end{aligned} \quad (11)$$

where $\sigma = 10, r = 28, b = \frac{8}{3}$, K_{ij} values represent the coupling strengths and $u_i(t)$ is a parameter through which we can perturb the i-th unit. We note that the Lorenz equations represent a chemical mechanism with many important kinetic features, e.g., rate determining steps followed by very fast reactions, cooperative catalysis, and some species to be in excess.[41] The units are assumed to be coupled through the y variables with coupling strength K_{ij}. In this example, all the coupling strength between the coupled unit (1-2 and 2-3) are set to 0.3. Our goal is to infer the network topology corresponding to the y couplings and in particular, estimate K_{ij} for all the outgoing links from unit 1. To do this task, we require that we are able to externally perturb the dynamics of y_1 and have access to measurement data for the variables $y_i(t)$.

To recover the outgoing connections from node 1, a step perturbation (Fig. 2(b)) is applied to node 1. As a result of the perturbation, the system displays a transient response, as shown in Fig. 2(c)-(e). Before the perturbation, the slope of the perturbed and the curvature of the connected nodes (2 and 3) are nearly zero. After the perturbation, as shown in Fig. 2(f), the slope of the perturbed node changes by 1, and the curvature (or second derivative) changes in nodes 2 and 3 by 0.30 and 0, respectively (see Fig. 2(g) and (h)). Thus, the inferred coupling strength (curvature change / slope change), is 0.30 and 0, which perfectly agrees with the existing coupling. (To recover the other links in

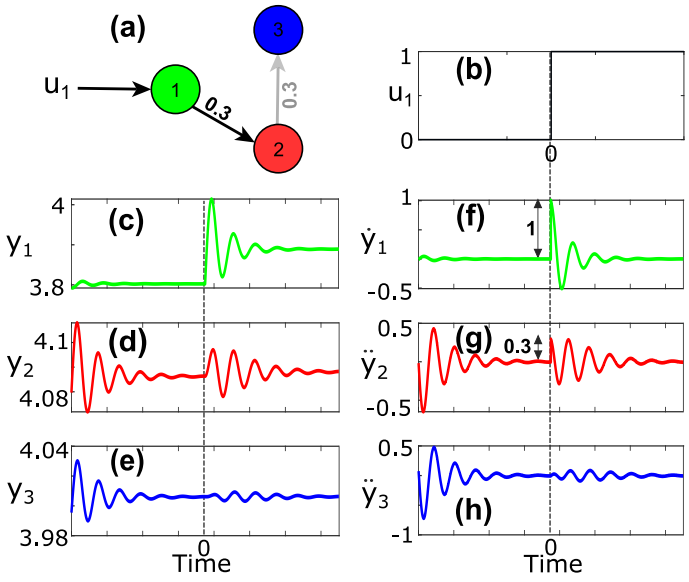

Fig. 2 Illustration of the proposed curvature analysis for inferring network connections. (a) A three node (directed chain) network of damped Lorenz systems with directed y -coupling. Perturbation u_1 is applied to node 1 to infer outgoing connections. The solid black edge is the one recovered through perturbing node 1 and the light grey edge will only by identified by perturbing node 2 (not shown in this figure). (b) The step input applied at node 1 at time $t = 0$. (c)-(e) Time series data of variable y at nodes 1,2, and 3. (f) The slope $\dot{y}_1(t)$ computed at node 1 using Euler approximation. (g)-(h) The curvature $\ddot{y}_i(t)$ for $i = 2,3$ computed at nodes 2 and 3 using Euler approximation. The ratio of the curvature of the coupled nodes ($\ddot{y}_i$, $i = 2,3$) with respect to the slope of the perturbed node $\dot{y}_1$ at the time of application of the step input reveals the outgoing connections of node 1 (as shown in (a)).

the network, perturbations should be applied to nodes 2 and 3; the results are shown in SI Section 2 Case 1). The methodology is not restricted to 2 or 3 node networks; as it is shown in SI section 2 Case 4, the coupling strengths can be completely recovered for a seven-node network as well. (This specific network will be also used in the experiments).

While the numerical algorithm was tested here with parameters where the dynamical system exhibits a stable stationary (equilibrium) point, the coupling strength formula in Eq. 10 is also valid with oscillatory or chaotic dynamics. This was confirmed in numerical simulations with the Lorenz system with chaotic system parameters in SI Section 2 Case 2. Similarly, the system can be perturbed with any parameter that uniquely affect the node dynamics; for example, in SI Section 2 Case 3 the network was reconstructed by perturbing parameter r instead of u.

3.3 Experiments with Electrochemical Networks

To verify the validity of the network reconstruction technique in practical settings, we performed experiments with the electrochemical dissolution of nickel in sulfuric acid electrolyte[42]. Under the applied conditions, the dissolution of Ni(s) to Ni^{2+}(aq) takes place through a NiO(s) oxide film. At large constant circuit potential, $V = 1.410$, the system exhibits complex dynamics, which include bistability, smooth and periodic oscillators, and chaos[43]. Here we use somewhat lower circuit potentials ($0.900\,\mathrm{V} \leq V \leq 1.100\,\mathrm{V}$), where the process settles to a steady state characterized by the measured electrode potential $E(t)$. As shown in Fig. 1(a), the electrodissolution takes place on a multielectrode array, where the chemical reaction takes place in (nearly) isolated units, which represent the node of the network. Coupling can be added through cross resistance (R_c) between the wires: When there is an electrode potential difference between the electrodes (due to different chemical environments), current can flow between the electrodes, which can promote additional nickel dissolution. In a typical experiment, a potential step was applied on one electrode (perturbed node), and the electrode potential time series was recorded for all the electrodes using potentiometry. The goal was to infer the coupling network topology for a wide range of networks and conditions.

Extraction of coupling strengths from experimental data

To extract the coupling strengths using Eq. (10), we need to compute the first- and second-order derivatives of the electrode potential time series using noisy experimental data. This was achieved by fitting a nonlinear function to the experimental time series, and calculating the change in the slope of the perturbed, and the change in the curvature of the coupled electrodes as follows.

For the perturbed system (indexed with subscript p), the experimental data could be fitted well with an exponential decay due to a potential step,

$$x_p(t) = A_p(1 - e^{-k_p t}), \tag{12}$$

where $x_p(t)$ is the offset corrected electrode potential, k_p is the rate constant of the decay, and A_p the amplitude response (i.e., the electrode potential change of the perturbed electrode when time goes to infinity).

Similarly, for the electrode potentials of the coupled system ($x_c(t)$), we used the fitting function given by

$$x_c(t) = A_c(1 - e^{-k_c t}(1 + k_c t + 0.5 k_m t^2)). \tag{13}$$

Note that this equation has an amplitude response (A_c) and a rate constant (k_c), but also includes a time-dependent multiplying factor, which describes the behavior of a typical coupled node through k_c and an indirectly coupled node through k_m. The mathematical forms of these fitting functions are further clarified in SI, Section 3.

Using these equations, coupling strength from the coupled to the perturbed node, i.e., the ratio of the curvature change of the coupled and the slope change of the perturbed electrode potentials can be obtained as:

$$K_f = \frac{A_c}{A_p}\frac{k_c^2 - k_m}{k_p}. \tag{14}$$

Eq. (14) clarifies how the impact of a perturbed node propagates through the network, and how time-scale separation is useful for network inference. In general, we can expect strong coupling between two nodes through two processes: (i) when a change of the state in a perturbed node (A_p) can have large impact on the coupled node (A_c) and (ii) when the coupled node reacts

quickly (large k_c), in comparison with the perturbed node (k_p). As the equation shows, the analysis of both of these processes is required for network inference. Note that the negative term in the equation (k_m) is essential because this term differentiates directly ($k_m = 0$) and indirectly ($k_c^2 = k_m$) coupled nodes. This term comes from the nonlinearity of the coupled waveform and reflects that indirectly coupled nodes typically react later to a perturbation in the network (and thus they depend on t^2 in Eq. (13)).

Finally, when the coupling is very weak, the step response of the coupled node (A_c) was very small; when it was smaller than three times the standard deviation of the signal before perturbation, the coupling strength was set to zero. (This helped eliminating overfitting of noisy data.)

Results with two coupled reactions

We first probed the accuracy of the technique by performing an experiment of two electrodes with homogeneous local dynamics, i.e., both electrochemical reactions have the same double layer charging constant ($R_{\mathrm{ind}}C_d$) determined by the double layer capacitance, and the externally variable individual resistance set to 10 kohm for both electrodes.

The experimental coupling strength (κ_{ij}) from electrode j to electrode i is the conductance per surface area, i.e., the

$$\kappa_{ij} = \frac{1}{R_c A_i} \tag{15}$$

where R_c is the coupling resistance and A_i is the surface area of ith electrode[44]. We applied a coupling strength of $\kappa_{21} = \kappa_{12} = 0.636\,\mathrm{mSmm^{-2}}$ and electrode 1 was perturbed with circuit potential step from $V(t) = 0.900V$ to $1.100V$ (see Fig. 3 (a)). The bottom panel of Fig. 3 (a) shows the electrode potential time series (black and blue dots for the perturbed and the coupled electrode, respectively) and the corresponding fits (red curve). From the analysis of the experimental data, the A_c, k_c, k_m, A_p and k_p values were estimated as 0.025 V, 72.25 $\mathrm{s^{-1}}$, -1.520 $\mathrm{s^{-1}}$, 0.038 V and 50.22 $\mathrm{s^{-1}}$ respectively, and the calculated extracted coupling strength, K_f was 68.40 $\mathrm{s^{-1}}$. Note that K_f cannot be directly compared to the κ_{12} because they represent the coupling at two different system levels. κ_{12} is the physical means of coupling, a conductance, that allows the flow current and thus enables the interactions. K_f is the coupling time-scale, which yields the results of the coupling in the time series.

If κ_{12} indeed responsible for the coupling extracted as K_f, we would find a linear relationship when κ_{12} is varied. We repeated the experiment for varying coupling strengths ($0.000\ \mathrm{mSmm^{-2}} \leq \kappa \leq 1.592\ \mathrm{mSmm^{-2}}$), and the corresponding K_f values are shown in Fig. 3(b). We found that, for $\kappa < 0.127\ \mathrm{mSmm^{-2}}$ the recovered coupling strength is zero ($K_f = 0\,\mathrm{s^{-1}}$); because of the apparent noise in Fig. 3, the very weak coupling cannot be detected. For a large range of intermediate coupling strengths, $0.127\ \mathrm{mSmm^{-2}} \leq \kappa \leq 0.636\ \mathrm{mSmm^{-2}}$, there is a nearly zero intercept linear relationship between κ and K_f. (Thus, the slope of this line, $100\,\mathrm{s^{-1}mS^{-1}mm^2}$ allows us to convert the two coupling strengths.)

Even for $\kappa > 0.636\ \mathrm{mSmm^{-2}}$, the coupling can be detected, but the coupling strength is underestimated and K_f shows a plateau

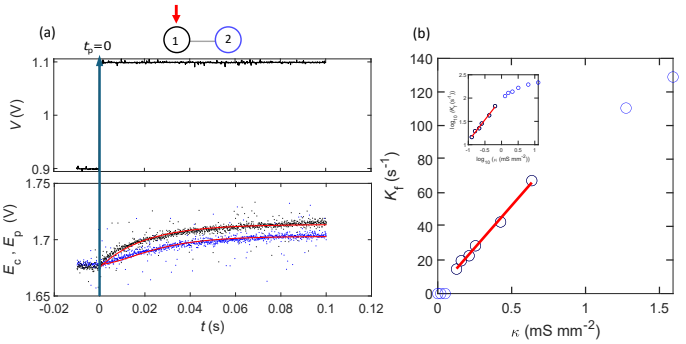

Fig. 3 Network reconstruction using two electrodes. (a) Perturbing the circuit potential of electrode 1 (at $t = t_P = 0$ s) and recording the electrode potentials to recover network with two nodes. Top: schematic of the experiment. Middle: Circuit potential vs time for electrode 1. Bottom: Electrode potential vs time for both electrodes during the perturbation experiment. $\kappa = 0.636\,\mathrm{mSmm^{-2}}$. $R_{\mathrm{ind}} = 10\mathrm{k}\Omega$. Black dots: electrode 1. Blue dots: electrode 2. Red line: fitted curve. (b) Extracted (K_f) vs. experimental (κ) coupling strengths. Red line: linear fit in the working range ($0.127\,\mathrm{mSmm^{-2}} \leq \kappa \leq 0.636\,\mathrm{mSmm^{-2}}$). The inset shows the logarithmic plot.

behavior for strong coupling (see inset in Fig. 3b). In this case, the coupling strength inference is limited by the time resolution of the experiments, and thus the amplitude responses ($A_p = A_c$) and the decay constants ($k_c = k_p$) are the same. The maximum recovered coupling can be estimated (using Eq. 14 with $k_m = 0$ as there are no indirect nodes) as $K_f = k_p \approx 50\,\mathrm{s^{-1}}$. This corresponds to about $\kappa = 0.5\ \mathrm{mSmm^{-2}}$. Indeed, we can see that the deviations from linear behavior occurred in this limiting range. We note that this maximum resolvable coupling limit could be expanded by choosing a perturbation with faster response time, i.e., larger k_p.

Recovering coupling between two highly heterogeneous node dynamics

The real strength of our proposed methodology is that it did not make any assumptions on similarity of the dynamics of the nodes. To demonstrate this, we performed network inference with two electrodes with very different individual resistances R_{ind} = 5 kohm and 15 kohm for electrodes 1 and 2, respectively. However, the same coupling coupling strength $\kappa_{12} = \kappa_{21} = 0.127\,\mathrm{mSmm^{-2}}$ was applied. As shown in Figs. 4(a-b), the perturbation experiments result in very different amplitude response and decay time constants, nonetheless, the recovered coupling constants were the same $K_f = 53\,\mathrm{s^{-1}}$ in both directions.

This experiment demonstrates that the coupling strength must be extracted by considering both the ratio of the amplitude response, and the ratio of the decay time-scales. Naively, one could calculate coupling strength based on the ratio of the coupled and the perturbed amplitude ratio (A_c/A_p). This coupling strength is shown Fig. 4c; for better comparison, the values are rescaled corresponding to the recovered coupling with respect to electrode 2 to 1. As shown in the figure, such inference would predict weaker (59 %) coupling from electrode 1 to 2 than in the opposing direction. Similarly, if one would calculate the coupling strength based on the ratio of the decay time constants (k_c/k_p), now the coupling would be predicted to be 67 % stronger for $1 \rightarrow 2$ than

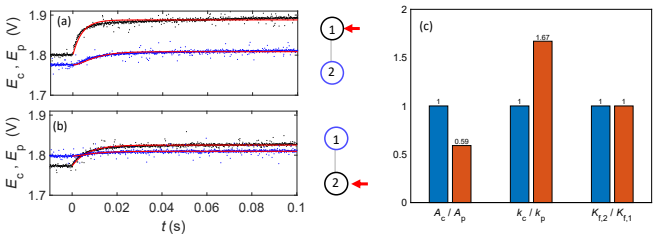

Fig. 4 Effectiveness of the perturbation technique to extract the coupling strengths between two electrodes with heterogeneous local dynamics, i.e., $R_{\mathrm{ind1}} = 5\,\mathrm{k\Omega}$ and $R_{\mathrm{ind2}} = 15\,\mathrm{k\Omega}$ for electrodes 1 and 2, respectively for an applied experimental coupling strength $\kappa = 0.127\,\mathrm{mSmm^{-2}}$. (a-b): Electrode potential time series for the perturbation in electrode 1 (a) and 2 (b). Notations are the same as in Fig.1(a). In panel (a) $A_c = 33$ mV, $k_c = 184\,\mathrm{s^{-1}}$, $k_m = 1.275\,\mathrm{s^{-1}}$, $A_p = 88$ mV, $k_p = 241.83\ \mathrm{s^{-1}}$. In panel (b), $A_c = 11.7$ mV, $k_c = 186\,\mathrm{s^{-1}}$, $k_m = 2.55\,\mathrm{s^{-1}}$, $A_p = 52.4$ mV, $k_p = 145.7\ \mathrm{s^{-1}}$. (c) Barplots of the rescaled extracted amplitude response, response time, and coupling strengths (see SI, section 3 for details)

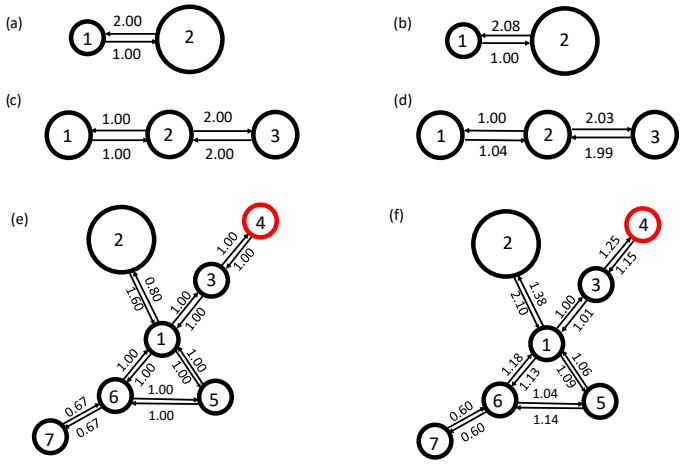

Fig. 5 Assessment of the wider applicability and accuracy of the network reconstruction technique in extracting coupling strength of complex networks by comparison of the experimental (left column) and reconstructed (right column) coupling strengths. (a-b) Asymmetric coupling with two electrodes induced by different electrode sizes. (c,d) Linear chain with three electrodes. (e,f) Seven node network with one asymmetrical link utilizing large electrode (node 2) and heterogeneity in node 4. For (a-b),(c-d) and (e-f) the link strengths were normalized with respect to the link from electrode $2-1$, $1-2$ and $3-1$ respectively where $X-Y$ denotes coupled node X and perturbed node Y.

$2 \to 1$. However, when we use the correct formula, the effect of the amplitude response and the decay time constants cancel each other and the coupling strengths are the same in both directions.

Results with complex networks

In addition, the versatility and robustness of the network inference framework was tested with complex networks shown in Fig. 5. For these experiments only the expected and the recovered network topology are shown; the detailed perturbation data are provided in the SI Section 4. (The coupling strengths are rescaled with respect to a recovered K_f value for one of the links as described on the figure caption.)

When the electrode has different surface area, asymmetrical coupling can occur with a large electrode driving the small electrode, as expected from Eq. 15. Fig. 5(a) shows such a network, with electrode 2 having twice the surface area of electrode 1. Owing to this surface area difference, asymmetrical coupling with electrode 2 to electrode 1 twice as strong as in the opposing direction was predicted; this prediction was confirmed in the inferred network with a ratio of 2.08.

Fig. 5(c) shows a three-electrode chain network, where the (symmetrical) coupling was twice as strong between electrodes 2 and 3, than electrodes 1 and 2. The network inference technique properly identifies the indirectly coupled electrodes 1-3 (zero coupling), and predicts the other coupling strengths with at most 4 % deviations from the expected coupling strengths (see Fig. 5(d)).

Finally, a seven-node network was constructed as shown in 5(e). The network consists of a densely coupled subnetwork (electrodes 1, 5, and 6), with end-nodes that have different surface areas (2 $\times$, node 2), heterogeneous node (electrode 4, $R_{\mathrm{ind}} = 20$ kohm instead of 10 kohm), and weaker coupling (node 7 to 6, 67 % of the typical strength). The inferred network could identify all the directly coupled nodes and differentiate them from the indirect (inferred zero) coupling (see Fig. 5(f)). All recovered coupling strengths, except between nodes 1 and 2, are symmetrical, as expected. Note that the asymmetry ratio was somewhat underestimated (1.5 instead of 2). The inferred network also properly predicted the weakened coupling strength between nodes 6 and 7. We thus see that the perturbation based technique as an excellent tool for recovering network topology; in particular, the method did not generate false positive links between indirectly coupled nodes, which is a notorious problem in network reconstruction with both the Granger causality and the model fitting frameworks.

4 Conclusions

We proposed a systematic framework for inferring the structure of chemical reaction networks using sequential node perturbations. By perturbing individual nodes (chemical species), the coupling strength between them is determined by comparing the curvature change in the trajectory of a coupled species with the slope change in the perturbed species. This approach doesn't assume specific local or interaction dynamics and accurately recovers the network reflecting the state during perturbation. If further information is needed about the network dynamics, one can make perturbations at different states, and explore the exact form of the coupling function from the state dependence of the coupling. When relatively small perturbations are applied, fitting functions could be used by which the slope and curvature changes can evaluated from fitting formulas. When there is strong coupling and thus large perturbations are needed, the slope and curvature changes are needed to be calculated numerically.

The application of the method revealed important insights about inferring networks. To recover the $N(N-1) = N^2 - N$ coupling strengths, one needs to evaluate the changes in slopes and curvatures in a given experiment, and all together to collect $N(4+6(N-1)) = 6N^2 - 2N$ data points. This data overhead ensures that the local and coupling dynamics can be effectively separated. In our view, an additional decrease in the required mini-

mum number of data points for network inference is only possible when further assumptions are made about the coupling topology (e.g., sparse network) or about the local/coupling dynamics.

The other important insight relates to intuition about how coupling affects species dynamics in the network. Perturbations lead to up-regulation in directly coupled species, with a lesser effect on indirectly coupled ones. Strong coupling results in faster responses from directly coupled species. However, species' sensitivity due to local dynamics can produce significant, rapid responses to minor perturbations. We showed that measuring both the up-regulation extent and the modified response time-scale is necessary to calculate coupling strength.

There are two major strengths of the perturbation based technique. First, as long as the slopes and curvatures can be faithfully extracted from the time series data, the network can be fully extracted. These changes may require new type of experimental design with high data acquisition rate and high signal-to-noise ratio. For example, with stopped flow technique comparing two experiments with different concentration of a species, one should be able to quantify the impact of the species on the rate equations of other observed species by comparing the change of the curvature of the observed kinetic trajectories. We note that while the proposed technique exhibits similarities to relaxation techniques, in particular to 'concentration jump' of fast reaction kinetics, however it also differs because it does not require an a-priori kinetic model and there is no requirement to apply small perturbation (and thus use linearized equations) to identify the model parameters. Moreover, different timescales in local kinetics is not a major complicating factor, because the main focus of the method is obtaining interactions among the nodes. The time-scales in coupling dynamics are exactly the inverse coupling strengths. At weak coupling, separation of experimental noise and the coupling effect can be problematic; in this case the signal-to-noise ratio needs to be improved (as in a classical kinetic investigations). With very strong coupling, the coupling strength can be detected, but its magnitude could be limited by the sensitivity of the kinetics of the perturbed node (i.e., the slope change). In this case, alternative perturbation needs to be explored (e.g., with other system parameters), which results in larger impact.

Second, hidden species or nodes do not affect the performance of the technique. In network inference with standard techniques, the hidden nodes pose a problem because the signals sent by hidden nodes directly or indirectly affect the dynamics and this impact is simulated with an effective network. In other words, the subnetwork is reconstructed concurrently for all the measured nodes. In contrast, our method traces the impact of one node on the other directly with pairwise analysis immediately after a perturbation – in such a short time after the perturbation, the effect of indirect connections are minimized. We note, however, because of the reasons stated above,the method would not reveal links to and from the hidden nodes, even when these links are important, for example, for an unobserved network hub node. In this case, the use of the reconstructed network could be somewhat limited, and thus further observations would be needed to simulate collective behaviors.

Here we presented an application with network of electrochemical reactions in which the dynamics settled to a far-from-equilibrium stationary state. The methodology can be applied to more complicated oscillatory or even chaotic dynamics as well. Numerically, we showed that the network topology of the chaotic Lorenz system can be inferred assuming the simulations can be started from the same initial conditions. In experiments, with coupled oscillators, such initial condition could be difficult to achieve. In these examples, phase resetting could be applied that set the phases of the oscillator to prescribed value[45].

In conclusion, the technique holds great promise in applications where high temporal resolution combines with low spatial resolution, for example, in multi-electrode array recordings of neural activities.

Author contributions

All authors contributed equally to this work.

Conflicts of interest

There are no conflicts to declare.

Data availability

The data supporting this article have been included as part of the Supplementary Information.

Acknowledgements

This work was supported in part by the NSF Awards ECCS-1810202 (JSL), CHE-1900011 (IZK), the AFOSR grant FA9550-21-1-0335 (JSL), and the National Institute of General Medical Sciences of the National Institutes of Health under award number R01GM157609 (JSL).

Notes and references

1 A. S. Mikhailov and V. Calenbuhr, *From cells to societies: models of complex coherent action*, Springer, Berlin ; New York, 2002.

2 M. Wen, E. W. C. Spotte-Smith, S. M. Blau, M. J. McDermott, A. S. Krishnapriyan and K. A. Persson, *Nat. Comput. Sci.*, 2023, **3**, 12–24.

3 M. Feinberg, *Foundations of chemical reaction network theory*, Springer, New York, NY, 2019.

4 S. Ronquist, G. Patterson, L. A. Muir, S. Lindsly, H. Chen, M. Brown *et al.*, *Proc. Natl. Acad. Sci. U.S.A.*, 2017, **114**, 11832–11837.

5 K. Kuritz, S. Zeng and F. Allgöwer, *IEEE Control Syst. Lett.*, 2018, **3**, 296–301.

6 A. Despons, Y. De Decker and D. Lacoste, *Commun. Phys.*, 2024, **7**, 224.

7 Y. Chen, Y. Su, C. Sui, W. Chen and B. Zhang, *Fuel Process. Technol.*, 2023, **242**, 107652.

8 Y. Orlova, P. D. Iedema and I. Kryven, Polymer Reaction Engineering X (PRE 10), 2018, p. 31.

9 M. L. Wong, A. Prabhu, J. Williams, S. M. Morrison and R. M. Hazen, *J. Geophys. Res.Planets*, 2023, **128**, e2022JE007658.

10 Z. Peng, J. Linderoth and D. A. Baum, *PLoS Comput. Biol.*, 2022, **18**, e1010498.

11 A. Hishida, T. Okada and A. Mochizuki, *PNAS Nexus*, 2024, **3**, pgad441.

12 V. A. Ranganath and I. Maity, *Angew. Chem. Int. Ed.*, 2024, **63**, e202318134.

13 R. Roszak, M. D. Bajczyk, E. P. Gajewska, R. Hołyst and B. A. Grzybowski, *Angew. Chem. Int. Ed.*, 2019, **58**, 4520–4525.

14 T. Okada and A. Mochizuki, *Phys. Rev. Lett.*, 2016, **117**, 048101.

15 T. Okada and A. Mochizuki, *Phys. Rev. E*, 2017, **96**, 022322.

16 O. Sinanoğlu, *J. Math. Phys.*, 1981, **22**, 1504–1512.

17 M. A. Budroni, K. Torbensen, S. Ristori, A. Abou-Hassan and F. Rossi, *J. Phys. Chem. Lett*, 2020, **11**, 2014–2020.

18 M. A. Budroni, K. Torbensen, O. L. Pantani, S. Ristori, F. Rossi and A. Abou-Hassan, *Chem. Commun.*, 2020, **56**, 11771–11774.

19 M. A. Budroni, G. Pagano, D. Conte, B. Paternoster, R. D'ambrosio, S. Ristori, A. Abou-Hassan and F. Rossi, *PCCP*, 2021, **23**, 17606–17615.

20 N. E. Kouvaris, M. Sebek, A. S. Mikhailov and I. Z. Kiss, *Angew. Chem. Int. Ed.*, 2016, **128**, 13461 – 13464.

21 I. Z. Kiss, Y. Zhai and J. L. Hudson, *Science (New York, NY)*, 2002, **296**, 1676 – 1678.

22 A. F. Taylor, M. R. Tinsley, F. Wang, Z. Huang and K. Showalter, *Science (New York, NY)*, 2009, **323**, 614 – 617.

23 W. Wang, I. Z. Kiss and J. L. Hudson, *Chaos*, 2000, **10**, 248–256.

24 H. Varela, C. Beta, A. Bonnefont and K. Krischer, *Phys. Chem. Chem. Phys.*, 2005, **7**, 2429–2439.

25 M. Wickramasinghe and I. Z. Kiss, *Plos One*, 2013, **8**, e80586.

26 M. R. Tinsley, S. Nkomo and K. Showalter, *Nat. Phys.*, 2012, **8**, 662 – 665.

27 L. Schmidt, K. Schönleber, K. Krischer and V. García-Morales, *Chaos*, 2014, **24**, 013102.

28 N. Tompkins, N. Li, C. Girabawe, M. Heymann, G. Ermentrout, I. R. Epstein and S. Fraden, *Proc. Natl. Acad. Sci. U.S.A*, 2014, **111**, 4397 – 4402.

29 S. Wang, E. D. Herzog, I. Z. Kiss, W. J. Schwartz, G. Bloch, M. Sebek, D. Granados-Fuentes, L. Wang and J.-S. Li, *Proc. Natl. Acad. Sci. U.S.A.*, 2018, **115**, 9300–9305.

30 J. Ren, W.-X. Wang, B. Li and Y.-C. Lai, *Phys. Rev. Lett.*, 2010, **104**, 058701.

31 C. J. Quinn, T. P. Coleman, N. Kiyavash and N. G. Hatsopoulos, *J. Comput. Neurosci.*, 2011, **30**, 17–44.

32 K. J. Friston, *Brain Connect.*, 2011, **1**, 13–36.

33 B. Barzel and A.-L. Barabási, *Nat. Biotechnol.*, 2013, **31**, 720–725.

34 S. Mukherjee and T. P. Speed, *Proc. Natl. Acad. Sci. U.S.A.*, 2008, **105**, 14313–14318.

35 M. Timme, *Phys. Rev. Lett.*, 2007, **98**, 224101.

36 M. Timme and J. Casadiego, *J. Phys. A: Math. Theor.*, 2014, **47**, 343001.

37 J. Casadiego, M. Nitzan, S. Hallerberg and M. Timme, *Nat. Commun.*, 2017, **8**, 2192.

38 B. N. Kholodenko, A. Kiyatkin, F. J. Bruggeman, E. Sontag, H. V. Westerhoff and J. B. Hoek, *Proc. Natl. Acad. Sci. U.S.A.*, 2002, **99**, 12841–12846.

39 E. Sontag, A. Kiyatkin and B. N. Kholodenko, *Bioinformatics*, 2004, **20**, 1877–1886.

40 E. Rihtar, T. Lebar, D. Lainscek, K. Kores, S. Lesnik, U. Bren *et al.*, *Nat. Chem. Biol.*, 2023, **19**, 64–71.

41 D. Poland, *Physica D*, 1993, **65**, 86–99.

42 J. Nawrath, M. C. Romano, M. Thiel, I. Z. Kiss, M. Wickramasinghe, J. Timmer, J. Kurths and B. Schelter, *Phys. Rev. Lett.*, 2010, **104**, 038701.

43 I. Z. Kiss, Z. Kazsu and V. Gáspár, *Chaos*, 2006, **16**, 033109.

44 M. Wickramasinghe, E. M. Mrugacz and I. Z. Kiss, *Phys. Chem. Chem. Phys.*, 2011, **13**, 15483–15491.

45 Y. Zhai, I. Z. Kiss, P. A. Tass and J. L. Hudson, *Phys. Rev. E*, 2005, **71**, 065202.

The data supporting this article have been included as part of the Supplementary Information.